SnS_2 quantum dots: facile synthesis, properties and applications in ultraviolet photodetector *

Yao Li(李尧)[1], Libin Tang (唐利斌)[1,2†], Rujie Li(李汝劼)[2,3], Jinzhong Xiang(项金钟)[1†], Kar Seng Teng[4] and Shu Ping Lau(刘树平)[5]

[1] *School of Materials Science and Engineering, Yunnan University, Kunming 650091, People's Republic of China*

[2]*Kunming Institute of Physics, Kunming 650223, People's Republic of China*

[3]*School of Physics, Beijing Institute of Technology, Beijing 100081, People's Republic of China*

[4] *College of Engineering, Swansea University, Bay Campus, Fabian Way, Swansea SA1 8EN, United Kingdom*

[5]*Department of Applied Physics, The Hong Kong Polytechnic University, Hong Kong, People's Republic of China*

Tin sulfide quantum dots (SnS_2 QDs) are *n*-type wide band gap semiconductor. They exhibit high optical absorption coefficient and strong photoconductive property in the ultraviolet and visible regions. Therefore, they have found many potential applications, such as gas sensors, resistors, photodetectors, photocatalysts and solar cells. However, the existing preparation methods for SnS_2 QDs were complicated and they required high temperature and high pressure environment, hence they were unsuitable for large-scale industrial production. An effective method for the preparation of monodispersed SnS_2 QDs at normal temperature and pressure will be discussed in this paper. The method is facile, green and low-cost. In this work, the structure, morphology, optical, electrical and photoelectric properties of SnS_2 QDs were studied. The synthesized SnS_2 QDs were homogeneous in size and exhibited good photoelectric performance. A photoelectric detector based on the SnS_2 QDs was fabricated and its *J-V* and *C-V* characteristics were also studied. The detector responded under λ=365 nm light irradiation and reverse bias voltage. Its detectivity stabilized at approximately 10^{11} Jones at room temperature. These results showed the possible use of SnS_2 QDs in photodetectors.

Keywords: SnS_2; quantum dots; photoelectric properties; photodetector
PACS: 78.67.Hc, 84.60.Jt, 85.60.Gz

1. Introduction

In recent years, there has been great interest in two-dimensional (2D) materials due to their high specific surface areas and excellent electronic properties. [1-3] Tin disulfide (SnS_2) is one of the members of Ⅳ:Ⅵ binary compounds in 2D metal chalcogenides. It is an n-type compound semiconductor with layered and hexagonal

* Project supported by the Equipment Pre-research Fund under the Equipment Development Department (EDD) of China's Central Military Commission (CMC) (No.1422030209), the Innovation Team Program of China North Industries Group Corporation Limited (NORINCO) Group (No.2017CX024) and the National Natural Science Foundation of China (No. 61106098，11864044).
† Corresponding author. E-mail: scitang@163.com
† Corresponding author. E-mail: jzhxiang@ynu.edu.cn

CdI_2 structures. [4] This structural unit is a two-layer sandwich structure, which comprised of hexagonal closely packed S^{2-} with Sn^{4+}. One Sn^{4+} and six S^{2-} form an octahedral coordination, which means S^{2-} is AB-AB hexagonal close packing and metal Sn^{4+} is between the double-deck S^{2-}. There is covalent bonding in the inner layer and weak van der Waals force between the layers. The bulk SnS_2 material exhibited non-toxicity and good chemical stability. Furthermore, the material can be produced at relatively low cost as its reactant is readily available. Hence, SnS_2 material has been studied for use in the fields of photoelectric detector, [5, 6] sensor [7] and lithium ion battery. [8]

Semiconductor QDs are quasi-zero-dimensional nanocrystals with electrons and holes confined in all three dimensions. [9, 10] Due to the confinement, the movement of the carriers is limited to a certain space resulting in an increase in electron kinetic energy. This leads to an increase in the material energy gap and the exciton energy, thus producing a quantum size effect where the band width is ultimately determined by the quantum dot's size. SnS_2 QDs, with size between 1 and 10 nm, have been applied in fields of photoelectric detector, [11] solar photocatalyst [12] and photovoltaic solar cell. [13] These devices demonstrated good detection capability, high sensitivity and high energy conversion efficiency.

Low-cost solution-based synthesis of colloidal semiconductor QDs has drawn increasing attention due to their applications in photodetectors. [14] The colloidal preparation methods of SnS_2 QDs include liquid-phase exfoliation (LPE), [15] solution thermal synthesis, [12] hot injection [13, 16] and wet chemistry methods. [17] The QDs prepared by colloidal chemistry are also known as colloidal quantum dots (CQDs). Colloidal chemistry method is a wet chemical method that used organic ligand molecules to wrap the surface of growing QDs to control particle agglomeration. [18] The general method involved the introduction of precursor solution quickly into a high-boiling-point organic solvent, which would generate a lot of nucleation centers. The coordination solvent molecules would dynamically adsorb on the surface of growing small particles to prevent or limit the growth of particles and to control the particle growing time in Qstwald ripening process (e.g. smaller particles have higher surface free energy, the small sol particles dissolved and redeposited on larger sol particles to achieve the growth of the macroparticles), hence resulting in monodispersed QDs. Small, homogeneous and high-quality QDs can be synthesized using this method by controlling the growth time. Colloidal QDs can be produced in different forms, such as solution, powder or film. Furthermore, it is easy to implement QDs surface engineering and can use different organic ligand molecules to envelop the surface of QDs to make it hydrophilic/hydrophobic. The preparation method of SnS_2 QDs in this work did not require high temperature and pressure processes. It involved mild reaction conditions and facile process to synthesize small and homogeneous SnS_2 QDs that showed good dispersion and stability in solvent.

2. Experimental

47T

2.1. Materials

The chemical reagents used in the experiments were purchased and used without further purification.

$SnCl_4 \cdot 5H_2O$ (AR), $Na_2S \cdot 9H_2O$ (AR 98.0%), $C_{12}H_{25}NaO_3S$ (AR 98.0%) were purchased from Tianjin Fengchuan Chemical Reagent Co., Ltd. (Tianjin, China). Ethanol (99.8% AR) and ethylene glycol (AR) were purchased from Chengdu Kelong Chemical Co., Ltd. (Sichuan, China).

2.2. Preparation of SnS_2 QDs

The preparation process of the SnS_2 QDs is shown in Figure 1(a). Below is the chemical equation of this experiment,

$$SnCl_4 + 2Na_2S = SnS_2 \downarrow + 4NaCl. \quad (1)$$

0.2 mol·L^{-1} Na_2S solution and 0.2 mol·L^{-1} $SnCl_4$ solution were prepared as the sulfur source and tin source respectively. The entire preparation process was performed on a heating plate at 50℃. To obtain 0.002g SnS_2, 548 μL $SnCl_4$ and 1073 μL Na_2S were introduced respectively to test tubes. Then 0.03 mol·L^{-1} $C_{12}H_{25}NaO_3S$ (as surfactant) were added respectively to Na_2S solution and $SnCl_4$solution (the ratio of the volume was 1:1), and mixed the two mixtures thoroughly. Subsequently, $SnCl_4$ mixed solution were dripped slowly into Na_2S mixed solution under constant stirring for 10 min until the reaction was completed. The products were centrifuged at 3000 rpm for 5 min. After centrifugation, the precipitate was reserved and a mixed solution of deionized water and ethanediol (the volume ratio was 1:1) was added and centrifuged again. This process was repeated twice. Once completed, the resultant yellow colored precipitate at the bottom of the solution was the desired SnS_2 QDs. Finally, ethylene glycol (as dispersant) was added to the yellow precipitate and collected via a pipette to a plastic test tube. The SnS_2 QDs were obtained.

2.3. Characterization Techniques

High-resolution Transmission Electron Microscopy (HRTEM) was performed on a JEM-2100 electron microscope operating at 200 kV. The Raman spectrum was obtained at ambient temperature on a Renishaw inVia Raman microscope with an argon-ion laser with an excitation wavelength of 514.5 nm. The Fourier-transform infrared (FTIR) spectra were measured by a NicoletiS10 infrared spectrometer using the KBr pellet technique. Optical properties were characterized by UV-Vis absorption spectra (SHIMADZU, Uv-1700) and fluorescence (Hitachi F-4500) spectrometers. Functional groups on the surface of the SnS_2 QDs were verified by X-ray photoelectron spectroscopy (XPS) using Al Kα radiation PHI VersaProbe II. X-ray diffraction (XRD) of the samples was measured using Rigaku D/Max-23 at room temperature. The surface morphology and roughness of SnS_2 QDs were investigated by scanning electron microscope (SEM) using Hitachi S3400 (Japan) and atomic force microscope (AFM) using SPA-400, respectively. The current density-voltage (*J*-*V*) characteristics were measured using Keithley 2400 source meter. The fluorescence effect was analyzed by a camera-obscura ultraviolet analyzer (ZF-7N). The images of the interdigital electrodes were observed using LEICA optical microscope (DM 2700M). The capacitance-voltage (*C*-*V*) curve was measured using a

semiconductor device analyzer (KEYSIGHT B1500A).

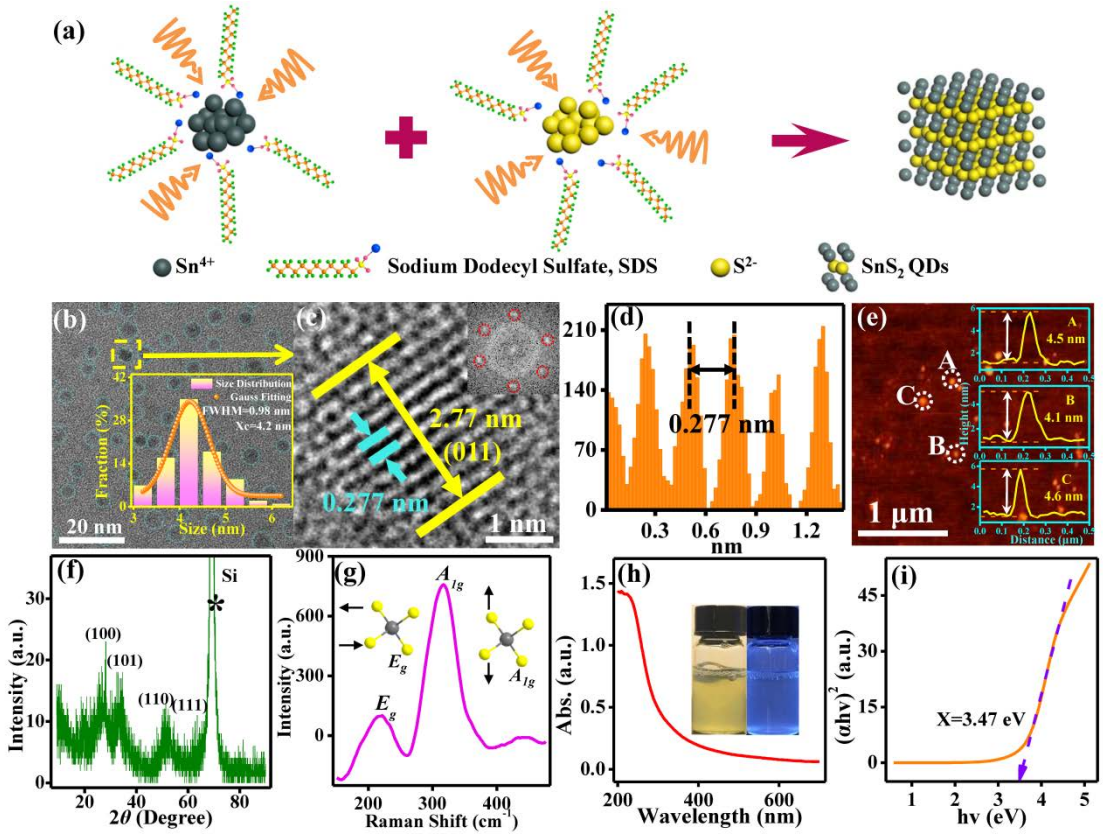

Fig. 1. (color online) (a) Schematic representation of the synthesis of SnS_2 QDs. (b) The TEM image of SnS_2 QDs and the size distribution of the SnS_2 QDs. (c) The HRTEM image of the SnS_2 QDs with lattice fringe spacing of 0.27 nm. (d) The line-profile analysis of the SnS_2 QDs as shown in (b). (e) AFM image of the SnS_2 QDs on Si substrate. (f) The XRD pattern of the SnS_2 QDs. (g) The Raman spectrum of the SnS_2 QDs on Si substrate with schematics of E_g and A_{1g} Raman vibrational modes. (h) UV-Vis absorption spectra of SnS_2 QDs aqueous solution. (i) Tauc plot for estimating the E_g of SnS_2 QDs.

3. Results and Discussion

3.1. Characterization of SnS_2 QDs

The SnS_2 QDs were characterized using TEM as shown in Fig. 1(b). The QDs were spherical in shape and their sizes were uniformly distributed. The size distribution of the SnS_2 QDs was analyzed as shown in the inset, which followed a Gaussian distribution as indicated by the fitting curve. The average diameter of the SnS_2 QDs was 4.2 nm with FWHM of 0.98 nm, which showed that the size distribution range of the QDs prepared by this method was narrow, hence demonstrating the uniformity of the QDs. Fig. 1(c) is a high-resolution TEM image of a typical single SnS_2 QD, which is indicated by a yellow square in fig. 1(b). The clear and bright lattice fringe demonstrated good crystallinity of the QDs. Fast Fourier-transform (FFT) was performed as shown in the inset, which revealed hexagonal crystal structures of the QDs. Fig. 1(d) is the line profile of the lattice

planes in Fig. 1(c) showing the inter-planar crystal spacing was 0.277 nm. [19] The morphology of SnS_2 QDs' thin film was studied using AFM as shown in Fig. 1(e). Height analysis of QDs A, B and C were shown in the inset. They were randomly selected and their height ranges from 4.1 nm to 4.6 nm, which were very close to the average size of the QDs (4.2 nm) obtained from the TEM image. Fig. 1(f) shows the XRD pattern of the SnS_2 QDs. The peak at 2θ=28.2°, 33.1°, 50.6° and 52.7° corresponded to lattice plane (100), (101), (110) and (111). [20] Si peak was observed in the XRD as the SnS_2 QDs was deposited on a silicon wafer. The Raman spectrum of the SnS_2 QDs is shown in Fig. 1(g). The vibrational modes of the QDs were studied. Two prominent peaks, such as E_g peak (~ 220 cm^{-1}) and A_{1g} peak (~ 317 cm^{-1}) were observed. Raman vibrational mode E_g corresponded to non-degenerate in-plane vibration mode, where as A_{1g} corresponded to Sn-S bonds of vertical out-of plane vibration. [21] The UV-Vis spectrum of SnS_2 QDs' aqueous solution is shown in Fig. 1(h), which showed an absorption peak at 225 nm in the ultraviolet range. This indicated a blue shift as compared to the absorption peak of 500 nm for SnS_2 bulk material. [22] Such phenomenon was attributed to the quantum confinement effect. The aqueous solutions of SnS_2 QDs are showed in the inset. On the left is the pale yellow solution of SnS_2 QDs in natural light and on the right is the SnS_2 QDs solution under 365 nm ultraviolet illumination, which demonstrated the fluorescence effect.

The bandgap energy (E_g) of the SnS_2 QDs can be obtained by the Tauc plot using [23]

$$\alpha h\nu = D(h\nu - E_g)^{1/2}, \tag{2}$$

where α is the absorption coefficient, D is a constant, $h\nu$ is the photon energy, and E_g is the bandgap energy. The bandgap energy (E_g) of SnS_2 QDs was estimated at 3.47 eV from the curve of $(\alpha h\nu)^2$ *vs* $h\nu$ in Fig. 1(i). The estimated value was larger than the bulk value of 2.31 eV [24] due to the quantum effect, the larger E_g makes SnS_2 QDs suitable for fabricating solar-blind UV detector. Under the effective-mass approximation, the size dependence of the bandgap of QDs can be represented as follows: [25]

$$E_g \approx E_{g(0)} + \frac{\hbar^2\pi^2}{2\mu R^2} - \frac{1.8e^2}{\varepsilon R} \tag{3}$$

where $E_{g(0)}$ is the bandgap of bulk SnS_2 (2.31 eV), $\hbar$ is the reduced Planck constant, μ is the reduced mass of excitation, R is the radius of SnS_2 QDs, e is the electron charge and ε is the dielectric constant of SnS_2 (20). [15] The calculated E_g value was 3.01 eV, which was close to the fitted value of 3.47 eV.

PL study of the as-prepared SnS_2 QDs solution was carried out using excitation wavelengths ranging from 360 nm to 400 nm. Fig. 2(a) shows the PL spectra of the QDs solution excited by various wavelengths. A wide PL peak can be observed at λ=465 nm. The normalized PL spectra of the QDs are also shown in the inset. Fig. 2(b) shows the PLE spectra of the QDs. A PLE peak was situated at λ=377 nm with different receiving energy (λ_{Em}), which revealed the different λ_{Em} has no effect on the peak position. The PLE results were in good agreement with the UV absorption

results. Normalized PLE spectra of the QDs are shown in the inset. The elemental

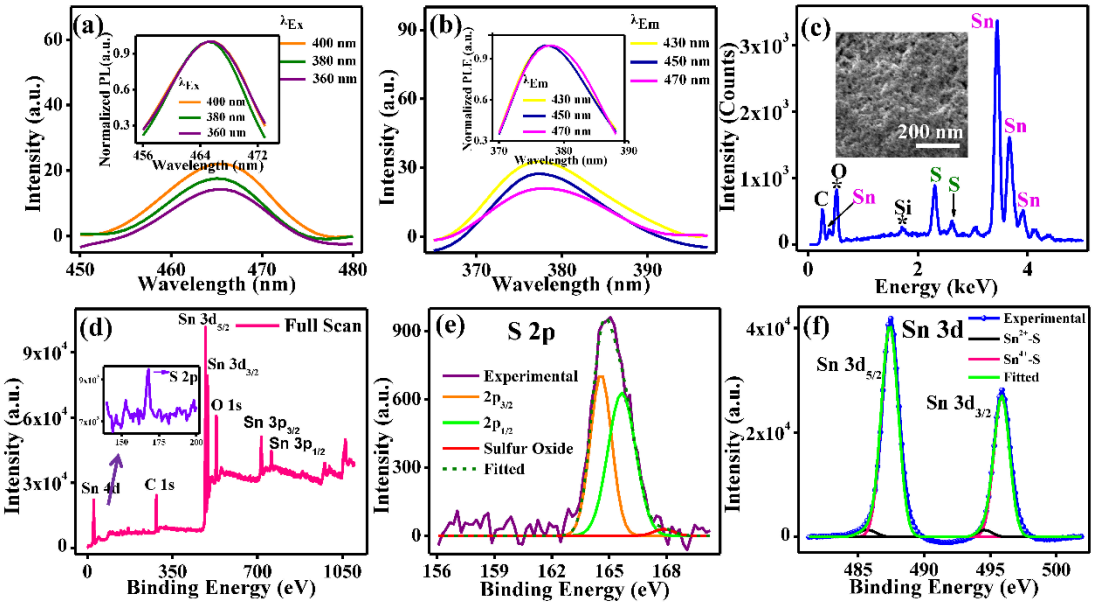

Fig. 2. (color online) (a) The PL spectra of SnS_2 QDs aqueous solution excited by various wavelengths and corresponding normalized PL spectra of the SnS_2 QDs. (b) The PLE spectra of SnS_2 QDs aqueous solution and normalized PLE spectra of the SnS_2 QDs. (c) EDS spectrum and SEM image of the SnS_2 QDs on a Si substrate (inset: SEM image). (d) The full-scan XPS spectrum of SnS_2 QDs. (e) The XPS S 2p spectrum of the SnS_2 QDs. (f) The XPS Sn 3d spectrum of the SnS_2 QDs.

analysis of the SnS_2 QDs was performed using EDS as shown in Fig. 2(c). The SEM image is shown in the inset of Fig. 2(c), and what we observed were aggregates of SnS_2 QDs. The S and Sn peaks indicated the presence of sulphur and tin, respectively. The small C and O peaks revealed the existence of a low-density of carbon and oxygen functional groups respectively, at the QDs prepared using this method. This could due to the surfactant, which was not removed entirely during the preparation process. The chemical composition of the SnS_2 QDs was analyzed using XPS. The full-scan XPS spectrum is shown in Fig. 2(d). The spectrum showed Sn $3d_{5/2}$ peak at 486.1 eV, Sn $3d_{3/2}$ peak at 495.5eV, Sn $3p_{3/2}$ peak at 716.6 eV, Sn $3p_{1/2}$ peak at 758.5 eV, Sn 4d peak at 25.8 eV, O 1s peak at 529.4 eV, and C 1s peak at 285.4eV. The S 2p peak at 167.7 eV can be observed in the inset. The presence of the C and O peaks could due to the C and O functional groups respectively, induced by the surfactant as well as exposure of the SnS_2 QDs to air. As shown in Fig. 2(e), S 2p core level peak was fitted with three peaks at 164.5 eV, 165.6 eV and 167.8 eV corresponded to S $2p_{3/2}$, S $2p_{1/2}$, and S-O respectively. [26] The Sn 3d core level peak is shown in Fig. 2(f), it was deconvoluted into two peaks, namely Sn $3d_{5/2}$ and Sn $3d_{3/2}$. It can be seen that the area of Sn^{4+} -S^{2-} was larger than the area of Sn^{2+} -S^{2-} in the fitted peaks, which indicated a very small amount of SnS in SnS_2 QDs. [27]

3.2. Characterization of Devices

The fabrication processes of the SnS_2-QDs-based photodetectors consisting of

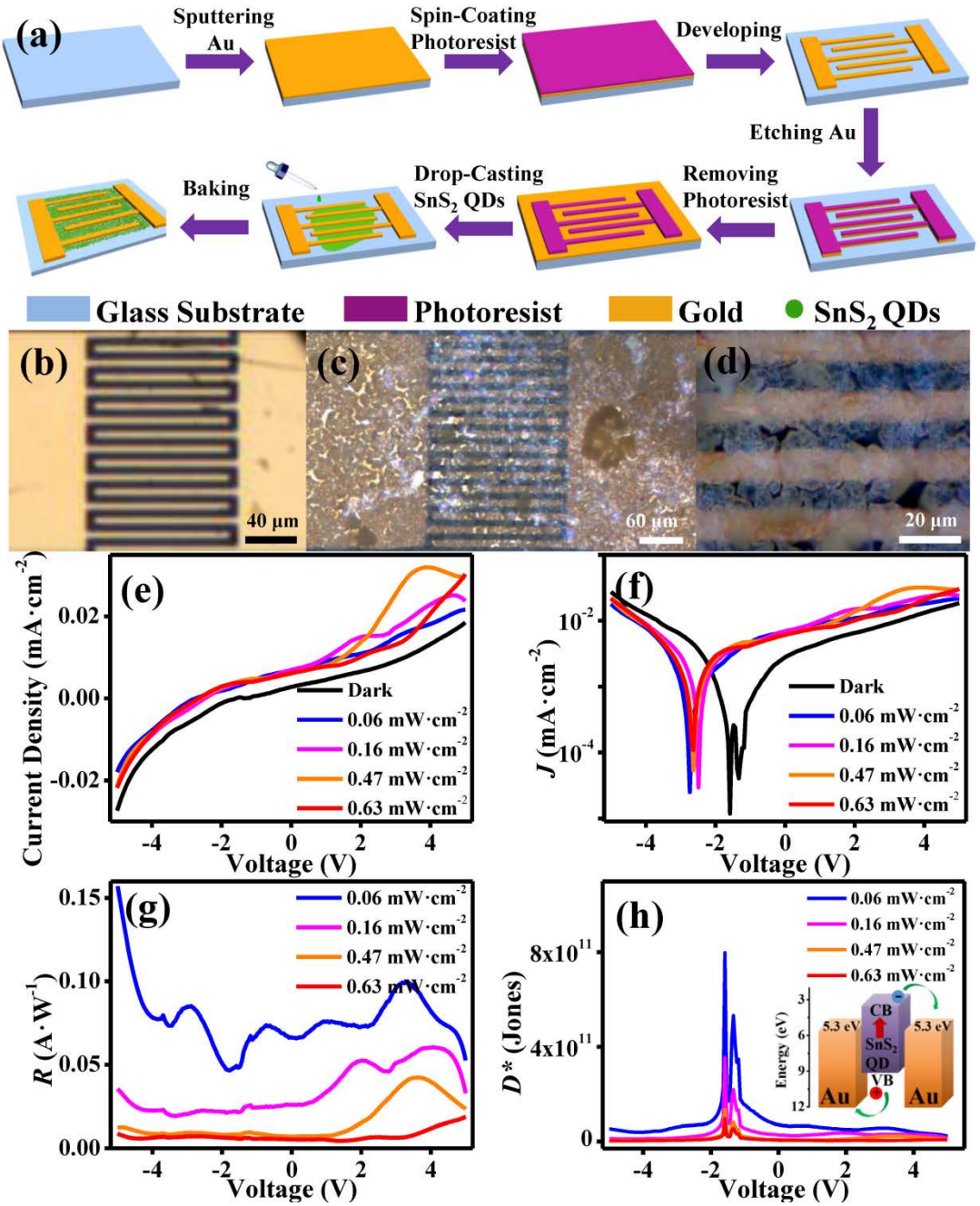

Fig. 3. (color online) (a) Schematic diagrams illustrating the fabrication process of the SnS_2 QDs photodetector. (b) The prepared interdigitated gold electrodes. (c) The SnS_2 QDs solution was drop-casted onto the interdigitated electrodes. (d) The enlarged image of the interdigitated electrodes under the microscope. (e) The *J*–*V* curves of the detector in the dark and under illumination at 365 nm with different light intensities. (f) log *(J)*-*V* curves. (g) *R* (Responsivity)-*V* curves. (h) *D** (Detectivity)-*V* curves (inset: the energy band diagram of the detector.).

interdigital gold electrodes are shown in Fig. 3(a). The SnS_2 QDs solution was drop-casted onto the interdigitated electrodes and dried at 50℃ on a heating plate in the air. The as-prepared interdigitated electrodes can be observed using an optical

microscope as shown in Fig. 3(b). Interdigitated electrodes covered with SnS_2 QDs can be observed at different magnifications in Fig. 3(c) and Fig. 3(d), which showed homogeneous and yellow QDs films. The *J–V* curve of the UV detector irradiated by λ=365 nm light under the conditions of 0 mW·cm^{-2}, 0.06 mW·cm^{-2}, 0.16 mW·cm^{-2}, 0.47 mW·cm^{-2} and 0.63 mW·cm^{-2} is shown in Fig. 3(e). The current density was increased under light irradiation, which suggested that the device responded to light and exhibited good photoelectric performance. Fig. 3(f) shows the log *(J)*-*V* curve, which showed the light current of the device was larger than the dark current. Therefore, the device is suitable for use in ultraviolet detection.

We discussed the responsivity (*R*) and detectivity (*D**) of the photodetector using the following expression：[28]

$$R = J_{ph} / P_{opt}, \tag{4}$$

$$D^* = \frac{R}{\sqrt{2q / J_d}}, \tag{5}$$

where J_{ph} is the photocurrent density, P_{opt} is the photo power density, q is the absolute electron charge (1.6×10^{-19} coulombs) and J_d is the dark current density. The value of *R* was relatively small in Fig. 3(g), however, the response rate increase as the reverse bias voltage increases. The *D** stabilized at 10^{11} Jones (1 Jones=1 cm·Hz$^{1/2}$·W^{-1}) and the detection rate increases as the light intensity decreases, indicating that the device is suitable for detecting light intensity. The energy band diagram of the detector is shown in the inset of Fig. 3(h), When ultraviolet light irradiates on the device, SnS_2 QDs absorb ultraviolet photons, and electrons excited from the valence band to the conduction band forming photogenerated electrons and photogenerated holes (excitons). Under the bias electric field, excitons are dissociated and collected by the electrodes, which is the UV photoelectric detection mechanism of SnS_2 QDs.

Resistance-temperature (*R*-*T*) characteristic of the detector based on SnS_2 QDs is is shown in Fig. 4(a). The resistance was about 10^6 Ω and it was obvious that the resistance increased linearly with increasing temperature. The resistivity (*ρ*) of the device was also calculated according to the electrode structure at different temperatures in order to understand the electrical properties of the QDs detector. The resistivity of the detector at different temperatures was calculated using the following formula:

$$\rho = R \cdot \frac{(N-1)\cdot\omega\cdot d}{l}, \tag{6}$$

where *R* is the resistance, *N* is the number of interdigitated electrodes, *ω* is the overlapping length of interdigitated electrodes, *l* is the spacing between the interdigitated electrodes and *d* is the film thickness. The *ρ*-*T* curve of the detector is shown in Fig. 4(b).

In general, the resistivity of a semiconductor decreases as the temperature increases. However, the observed resistivity of the SnS_2 QDs based detector is different from the conventional semiconductors. For semiconductor with impurity, the

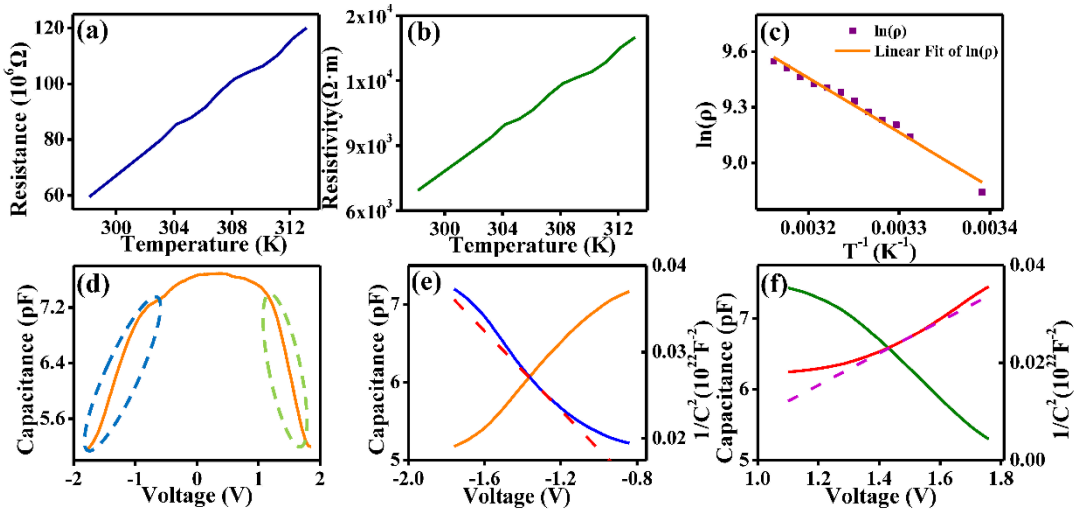

Fig. 4. (color online) (a) The *R*-*T* curve of the detector based on SnS_2 QDs. (b) The ρ-*T* curve of the detector based on SnS_2 QDs. (c) The ln(ρ)-1/*T* curve of the detector based on SnS_2 QDs. (d) The *C*–*V* curves of the SnS_2 QDs detector. (e) The *C*-*V* curves and plots of $1/C^2$ vs. V for the detector which was divided into two parts, corresponding to (e) and (f), respectively.

resistivity increases with temperature near room temperature [29] and the SnS_2 QDs based detector shows similar property in this aspect. In the above EDS and XPS spectra, it is evident that oxygen is present in the SnS_2 QDs and oxygen could act as impurity, hence the SnS_2 QDs based detector exhibits similar behavior as semiconductors with impurity. The ln(ρ)-1/*T* curve shown in Fig. 4(c) can be explained using the following expressions:

$$\rho = E \cdot \exp\left(E_a / k_B \cdot T\right), \tag{7}$$

where E is a pre-exponential factor, E_a is the thermal activation energy, k_B is the Boltzmann factor and T is absolute temperature. Taking natural log on both sides of equation (7):

$$\ln\left(\rho\right) = \ln\left(E\right) + E_a / \left(k_B \cdot T\right). \tag{8}$$

The unary linear regression of the values ln(ρ)-1/*T* was carried out in equation (7), which is shown in Fig. 4(c). The thermal activation energy and index factor of the detector can be calculated with the obtained intercept and slope, respectively. Table 1 shows the respective data and calculated values. The regression coefficient in the table 1 is 0.98, which is very close to 1, indicating that ln(ρ) and 1/*T* has a good linear relationship and the large pre-exponential factor resulted in a large resistivity of the device.

The *C*–*V* plots and the variation of $1/C^2$ at room temperature under 1 kHz illumination at voltage range from -2 V to 2 V are shown in Fig. 4(d). Under a bias, The *C*–*V* relationship can be expressed as: [30]

Table 1. Relative parameters of the device, the calculated value of the thermal activation energy and the index factor.

Intercept (ln(E))/ Ω·m	Slope(｜E_a/k_B｜)	Regression coefficient	E/ Ω·m	｜E_a｜/eV
22.96	4.19×10^3	0.98	9.33×10^9	0.36

$$C^{-2} = \frac{2(V_{bi} - V)}{q\varepsilon_0\varepsilon_r NF^2} \tag{9}$$

where V_{bi} is the built-in potential at zero bias, ε_0 is the permittivity of a vacuum, ε_r is the relative permittivity of the material, N is the carrier concentration in the depletion layer and F is the photosensitive area (3.33×10^{-4} cm^2). The x-intercept is V_{bi}, and N can be calculated from the slope of the linear part of the curve between $1/C^2$ and V:

$$N = \frac{-2}{q\varepsilon_0\varepsilon_r F^2}\left[\frac{\partial\left(C^{-2}\right)}{\partial V}\right]^{-1} \tag{10}$$

where ε_r for SnS_2 QDs is 20. [15]

The depletion layer width (W_d) is expressed as:

$$W_d = \left[\frac{2\varepsilon_0\varepsilon_r\left(V_{bi} - V\right)}{qN}\right]^{1/2} \tag{11}$$

The change in capacitance on the left and right parts of the curve in Fig. 4(d), which were circled using different color have been analyzed in Fig. 4(e) and (f), respectively. Table 2 shows the data obtained. As the structure of Au/SnS_2 QDs/Au devices has no polarity, the *C*–*V* curve is symmetrical. The values of V_{bi}, N and W_d are similar under positive and negative bias. Compared to other photodetectors, [31] the values of V_{bi}, N and W_d of the detector based on SnS_2 QDs are similar to graphene QDs based photovoltaic detector. Graphene based heterojunctions have been widely studied, [32-34] it is found that different heterojunctions formed by different materials or different conductive types (*n*-type or *p*-type) materials result in different *C*-*V* curve characteristics. For asymmetric unipolar heterojunctions, *C*-*V* curves are mostly monotonous, while for non-polar symmetrical heterojunctions, *C*-*V* curves are symmetric with V = 0 V. Apparently our Au/ SnS_2 QDs/Au device belongs to the last case (symmetric *C*-*V* curve).

Table 2. The built-in potential, carrier concentration and depletion layer width of SnS_2 QDs heterojunction at 1 kHz.

SnS_2 QDs	V_{bi} / V	N / 10^{18} cm^{-3}	W_d / nm (V=0)
Negative bias	0.95	1.36	15.44
Positive bias	0.74	1.43	11.44

4. Conclusion

In conclusion, homogeneous and monodispersed SnS_2 QDs were synthesized for

the first time using a low-cost, facile, green and effective method under ambient pressure at temperature lower than 80℃. The size and morphology of the SnS_2 QDs were characterized using TEM and AFM techniques. SnS_2 QDs have small dimension with an average particle size of 4.2 nm and exhibited good crystallinity. Absorption of the SnS_2 QDs solution was observed in the ultraviolet band. The performance of the photodetector based on SnS_2 QDs was stable as the *J-V* curve remained unchanged in repeating measurements. Under λ=365 nm illumination, the response rate (*R*) of the photodetector was greater than 0.10 $A \cdot W^{-1}$, and the detection rate (*D**) was about 10^{11} Jones. This work demonstrated the use of the SnS_2 QDs prepared using the facile method in UV photodetector, which showed excellent performances.

References

1. Lee M J, Ahn J H, Sung J H, Heo H, Jeon S G, Lee W, Song J Y, Hong K H, Choi B, Lee S H and Jo M H 2016 *Nat. Commum.* **7** 12011
2. Buscema M, Barkelid M, Zwiller V, Herre S J V D Z, Steele G A and Gomez A C 2013 *Nano Lett.* **13** 358
3. Li X, He D W, Wang Y S, Hu Y, Zhao X, Fu C and Wu J Y 2018 *Chin. Phys. B* **27** 056104
4. Xia J, Zhu D D, Wang L, Huang B, Huang X and Meng X M 2015 *Adv. Funct. Mater.* **25** 4255
5. Zhou X, Gan L, Zhang Q, Xiong X, Li H Q, Zhong Z Q, Han J B and Zhai T Y 2016 *J. Mater. Chem. C* **4** 2111
6. Zhou X, Zhang Q, Gan L, Li H Q and Zhai T Y 2016 *Adv. Funct. Mater.* **26** 4405
7. Ou J Z, Ge W Y, Carey B, Daenake T, Rotbart A, Shan W, Wang Y C, Fu Z Q, Chrimes A F, Wlodarski W, Russo S P, Li Y X and Kalantar-zadeh K 2015 *ACS Nano* **9** 10313
8. Seo J, Jang J, Park S, Kim C, Park B and Cheon J 2008 *Adv. Mater.* **20** 4269
9. Klimov V I, Mikhailovsky A A, Xu Su, Malko A, Hollingsworth J A, Leatherdale C A, Eisler H J and Bawendi M G 2000 *Science* **290** 314
10. Tang Jing and Xu X L 2018 *Chin. Phys. B* **27** 027804
11. Gao L, Chen C, Zeng K, Ge C, Yang D, Song H S and Tang J 2016 *Light: Sci. & Appl.* **5** e16126
12. Yuan Y J, Chen D Q, Shi X F, Tu J R, Hu B, Yang L X, Yu Z T and Zou Z G 2016 *Chem. Eng. J.* **313** 1438
13. Tan F R, Qu S C, Wu J, Liu K, Zhou S Y and Wang Z G 2011 *Nanoscale Res. Lett.* **6** 298
14. Qiao B, Zhao S L, Xu Z and Xu X R 2016 *Chin. Phys. B* **25** 098102
15. Fu X, Ilanchezhiyan P, Kumar G M, Cho H D, Zhang L, Chan A S, Lee D J,Panin G N and Kang T W 2017 *Nanoscale* **9** 1820
16. Truong N T N and Park C 2016 *Electron. Mater. Lett.* **12** 308
17. Tsukigase H, Suzuki Y, Berger M H, Sagawa T and Yoshikawa S 2011 *J. Nanosci. Nanotechnol.* **11** 3215
18. Yin Y and Alivisatos A P 2005 *Nature* **437** 664
19. Zhai C X, Du N and Yang H Z D 2011 *Chem. Commun.* **47** 1270

20. Tu J R, Shi X F, Lu H W, Yang N X and Yuan Y J 2016 *Mater. Lett.* 185 303
21. Bharatula L D, Erande M B, Mulla I S, Rout C S and Late D J 2016 *RSC Adv.* **6** 105421
22. Tan F R, Qu S C, Zeng X B, Zhang C S, Shi M J, Wang Z J, Jin L, Bi Y, Cao J, Wang Z G, Hou Y B, Teng F and Feng Z H 2010 *Solid State Commun.* **150** 58
23. Lin C X, Zhu M S Q, Zhang T, Liu Y F, Lv Y C, Li X J and Liu M H 2017 *RSC Adv.* **7** 12255
24. Yuan H, Sutter E, Sadowski J T, Cotlet M, Monti O L A, Racke D A, Neupane M R, Wickramaratne D, Lake R K, Parkinson B A and Sutter P 2014 *ACS Nano* **8** 10743
25. Satoh N, Nakashima T, Kamikura K and Yamamoto K 2008 *Nat. Nanotechnol.* **3** 106
26. Li X L, Chu L B, Wang Y Y and Pan L S 2016 *Mat. Sci. Eng. B* **205** 46
27. Ham G, Shin S, Park J, Lee J, Choi H, Lee S and Jeon H 2016 *RSC Adv.* 6 54069
28. Gong X, Tong M H, Xia Y J, Cai W Z, Moon J S, Cao Y, Yu G, Shieh C L, Nilsson B and Heeger A J 2009 *Science* **325** 1665
29. Liu E K, Zhu B S and Luo J S 2011 *The Physics of Semiconductors*, 7th edn. p. 111 (in Chinese)
30. Ramar M, Suman C K, Manimozhi R, Ahamad R and Srivastava 2014 *RSC Adv.* **4** 32651
31. Zhao J H, Tang L B, Xiang J Z, Ji R B, Hu Y B, Yuan J, Zhao J, Tai Y J, Cai, and Y H 2015 *RSC Adv.* **5** 29222
32. Miao X C, Tongay S, Petterson M K., Berke K, Rinzler A G., Appleton B R. and Hebard A F. 2012 *Nano Lett.* **12** 2745
33. Shivareman S, Herman L H., Rana F, Park J and Spencer M G. 2012 *Appl. Phys. Lett.* **100** 183112
34. Singh A, Uddin M A, Sudarshan T and Koley G 2014 *Small* **10** 1555